Available online at www.sciencedirect.com

ScienceDirect

Energy Procedia 148 (2018) 218–225

Energy Procedia

www.elsevier.com/locate/procedia

73rd Conference of the Italian Thermal Machines Engineering Association (ATI 2018), 12-14 September 2018, Pisa, Italy

Secondary flow and radial mixing modelling for CFD-based Through-Flow methods: an axial turbine application

Martina Ricci[a,*], Roberto Pacciani[a], Michele Marconcini[a], Andrea Arnone[a]

[a]*Department of Industrial Engineering, University of Florence, Via di S. Marta, 3, Florence 50139, Italy*

Abstract

The paper presents the theoretical bases and an application of a CFD-based Through-Flow model. The code solves the axisymmetric Euler equations and takes into account the effect of tangential blockage and body force. It inherits its numerical scheme from a state-of-the-art CFD solver (TRAF code). Blade body forces are calculated directly from the tangency condition to the meridional flow surface, which is iteratively adapted during the time-marching procedure. Dissipative forces are computed through a realistic distribution of entropy along streamlines. Both secondary flow and tip leakage effects on the meridional flow-field are included through the adoption of a concentrated vortex model, while the corresponding loss contributions are evaluated from correlations. Also, a radial mixing model considering both turbulent diffusion and spanwise convection is implemented.

The accuracy of the method is assessed by comparison with CFD calculations and experimental data on the transonic CT3 turbine stage tested in the framework of the TATEF2 European project. A good agreement in terms of overall performance and radial distributions is achieved for both design and off-design operating conditions.

Keywords: Through-Flow model; Axisymmetric Euler equation; Secondary flows; Radial mixing; Turbomachinery.

1. Introduction

For the design of multistage turbomachinery several tools are generally employed in a hierarchical way. They can be grouped into three categories: one-dimensional ones, such as the Mean-Line models, two-dimensional or quasi-three-dimensional ones, such as Blade-to-Blade or Through-Flow, three-dimensional steady or unsteady viscous models based on Computational Fluid Dynamics (CFD). Throughflow methods traditionally represent a key tool for turbomachinery design. In preliminary stages, they are able to provide the designer with realistic spanwise distributions of flow parameters [15]. Recently, numerical methodologies borrowed from CFD approaches have be-

*Corresponding author. Tel.: +39-055-275-8784 ; fax: +39-055-275-8755
E-mail address: martina.ricci@unifi.it

1876-6102
10.1016/j.egypro.2018.08.071

gun to be exploited to solve the axisymmetric Euler [19] and Navier-Stokes [17], [20] equations in the framework of time-marching throughflow solvers. Although heavily dependent on empirical correlations for viscous losses and deviations, just like traditional approaches based on the streamline curvature model [18], such methods have no major difficulties in dealing with subsonic, transonic or supersonic flow regimes.

With the progress in turbomachinery performance, optimization techniques aimed at controlling the flow details have become increasingly important in any stage of the design process. There is a strong industrial interest in improved tools in order to effectively accomplish this goal.

The paper presents a novel, CFD-based throughflow method. It solves the axisymmetric Euler equations with tangential blockage and body forces and inherits its numerical scheme from a state-of-the-art CFD solver (TRAF code [2]). Blade body forces are calculated directly from the tangency condition to the meridional flow surface, which is iteratively adapted during the time-marching procedure to address incidence and deviation effects. Dissipative forces are computed through a realistic distribution of entropy along streamlines. The methodology includes a general framework for introducing the average effect of three-dimensional flow features, like secondary flows and tip leakage effects, in the context of the axisymmetric flow assumption [14]. A radial mixing model, which accounts for background turbulent diffusion and deterministic spanwise transport due to secondary flows is also implemented.

The effectiveness of the models introduced are evaluated by studying the CT3 turbine stage tested in the framework of the TATEF2 (Turbine Aero-Thermal External Flows) European project. Three-dimensional CFD simulations and experimental data are available for design and off-design operating conditions. Transonic flow regime, low aspect ratio geometry and rotor tip clearance makes it an inspiring and stimulating configuration for assessing the accuracy and reliability of the throughflow procedure. The comparison between throughflow prediction and experimental data will be discussed in terms of overall performance and flow quantities's spanwise distribution.

Nomenclature

b	tangential blockage factor
d	dissipative force magnitude
f	blade body force magnitude
H	specific total enthalpy
J	Jacobian of the coordinate transformation
p	pressure
s	specific entropy
u, v, w	axial, radial, tangential velocity
x, r, θ	cylindrical coordinates
Γ	stream surface
ϵ	mixing coefficient
k_t	eddy thermal conductivity
μ_t	eddy viscosity
ξ, η	curvilinear coordinates
ρ	fluid density

2. Governing equations

A suitable model for the meridional analysis of turbomachinery can be obtained by circumferentially averaging the system of the Euler equations in cylindrical coordinates. The source terms, that arise as a result of the averaging process in bladed regions of the meridional flowpath, can be recast in the form of tangential blockage dependent terms and body forces responsible for the flow deflection. To this, it is customary to add a dissipative body force field which is used to model viscous losses.

The continuity, momentum and energy equations written in conservative form and mapped in a curvilinear, body fitted coordinate system are:

$$\frac{\partial bJ^{-1}U}{\partial t} + \frac{\partial bJ^{-1}F}{\partial \xi} + \frac{\partial bJ^{-1}G}{\partial \eta} = bJ^{-1}S + J^{-1}S_b + J^{-1}S_f, \tag{1}$$

where U is the conservative variables vector, F and G are the inviscid flux vectors. For example, in η direction:

$$G = \left[\rho V, \rho V u + p\eta_x, \rho V v + p\eta_y, \rho V w, \rho v H\right]^T. \tag{2}$$

On the right hand side:

$$S = \left[-\rho v, -\rho u v, \rho w^2 - \rho v^2, -\rho v H\right]^T, \tag{3}$$

is a source term vector arising from the formulation of the equations in cylindrical coordinates, while:

$$S_b = \left[0, p\frac{\partial b}{\partial x}, p\frac{\partial b}{\partial r}, 0, 0\right]^T, \quad S_f = \left[0, \rho f_x - \rho d_x, \rho f_r - \rho d_r, \rho f_\theta - \rho d_\theta, \rho(f_\theta - d_\theta)\Omega r\right]^T. \tag{4}$$

represent the source term vectors which account for the variation of tangential blockage in the blade passage, and for the components of the blade body forces, f, and the dissipative force, d.

The throughflow code inherits its numerical scheme from the steady release of a CFD solver, the TRAF code [2]. The system of governing equations (1) is solved via a time-marching procedure, with an explicit four-stage Runge-Kutta scheme. Residual smoothing, local time-stepping and multi-grid are employed to speed up convergence to the steady state solution [14]. A cell centered finite volume scheme is adopted to discretize the computational domain. The artificial dissipation model available in the code is the one introduced by Jameson et al. [10].

2.1. Blade and dissipative body force model

The blade body force field is intended to produce flow turning in the relative frame of reference, without generating losses. It is then assumed to be orthogonal to the flow surface and null in non-bladed regions. The blade body force magnitude can be determined by assuming that the deflection of the meridional (S2) stream surface, which represents the average path of the flow, is equal to the one of the mean surface of the blade. In analysis problems, the blade mean surface can be obtained, from the real blade geometry, in the functional form $\Gamma(x, r)$, or, equivalently, in the implicit form $\varphi(x, r, \vartheta) = \vartheta - \Gamma(x, r)$. The blade force components can be written as: $f_x = -f\frac{\partial \Gamma}{\partial x}$, $f_r = -f\frac{\partial \Gamma}{\partial r}$, $f_\vartheta = \frac{f}{r}$.

The value of the relative tangential velocity required to obtain the correct flow deflection can be obtained from the flow tangency condition to the mean blade surface in the relative frame of reference:

$$\tilde{w} = \Omega r + ur\frac{\partial \Gamma}{\partial x} - vr\frac{\partial \Gamma}{\partial r} \tag{5}$$

The body force magnitude f and the tangential velocity $\tilde{w}$ are related through the angular momentum equation, which gives:

$$f_\vartheta r = f = u\frac{\partial r\tilde{w}}{\partial x} + v\frac{\partial r\tilde{w}}{\partial r} \tag{6}$$

Equations (5) and (6) allow a direct calculation of the blade body force field, once the blade mean surface is known. Moreover equation (6) can be directly used also for design purposes, where an angular momentum distribution $r \cdot \tilde{w}(m, r)$ is typically prescribed between blade row inlet and outlet.

In the actual operation of turbomachines the flow direction at the inlet and outlet of a given blade row does not follow the camberline angle at the airfoil leading and trailing edge due to incidence and deviation effects. As a consequence, the actual stream surface does not coincide with the mean blade surface, and their differences due to incidence and deviation must be accommodated with a suitable treatment. In the present work the adaptive formulation for the mean stream surface proposed in [14] is employed.

Viscous losses are introduced in the system of equations (1) via a distributed loss model (e.g. Denton [5]). According to this, a dissipative force per unit volume, d, is added to the source term vector (4). Such a force is assumed to be aligned with the flow and opposite to it, so that it only results in loss generation. The correspondent entropy increase can be related to the dissipative force via the Crocco's theorem:

$$d = T\nabla s \cdot t \tag{7}$$

where t is the unit vector tangent to the streamline. The entropy rise across a blade row is computed via loss correlations. It is then distributed along streamlines by using a law that closely follows the ones predicted with viscous, three-dimensional, CFD calculations [14].

3. Secondary flow model

Secondary flow features are modelled in the circumferentially averaged flow-field as additional flow distorsions and losses. The details of the model can be found in [13], and therefore only a brief description is given here. Flow distortions are introduced in the throughflow procedure via a transverse velocity field associated with secondary vortices. The secondary velocity components, after being circumferentially averaged, are represented in terms of Lamb-Oseen type vortices. The vortex intensity, or circulation, is calculated from a suitable secondary vorticity distribution. In the present work, the classic formulation proposed by Hawthorne [9] for the streamwise vorticity at the trailing edge has been adopted. Such a vorticity contribution is assumed as concentrated in the vortex center and not distributed in the blade passage like in the classical secondary flow theory.

The vortex core length is calculated from the secondary flow penetration depth H. Such a quantity is commonly used in correlations to characterize the span fractions from hub and tip endwalls that are affected by secondary vortices. In this work the correlation suggested by Benner [3] has been used for that purpose. It is implied that at a spanwise distance from the endwall equal to H, the secondary velocity component is reduced by 5% of its maximum value and the vortex core length is calculated accordingly. Finally, the secondary velocity component is projected in the tangential direction to obtain a tangential velocity, $\tilde{w}$, which is then used in equation (6) to generate an additional body force that produces the spanwise distribution of secondary deviation.

Secondary losses are estimated via correlations, like the ones by Benner [3] or Kacker and Okapuu [11]. Secondary loss coefficients are converted in entropy rise values, where local flow conditions at the endwalls are used for this purpose. Such values are then distributed in the spanwise direction by a function that best represents the dissipation in a Lamb-Oseen vortex and that closely matches the results of viscous, three-dimensional, CFD calculations.

4. Tip clearance model

Tip clearance effects could be, in principle, accounted for in the throughflow procedure in a fashion similar to that of secondary flows. Unfortunately the available correlations for the tip vortex penetration depth in the spanwise direction and for the induced loss in flow turning by the blade row are characterized by a high level of empiricism and unsatisfactory agreement between different formulations [16], [21]. Therefore it was decided to model tip leakage effects in terms of source and sink flux vectors and additional losses.

The sink and source terms are conceived in a form that conserves mass and energy while changing the momentum components in order to mimic tip leakages effects. They are introduced in the streamwise row of computational cells adjacent to the tip endwall in rotor blades. The height of those cells is enforced to be equal to the tip gap height by the grid generation procedure. For the sink terms the values of pressure, density and temperature are assumed equal to that of the main flow. For the source terms pressure and temperature are assumed equal to that of the main flow while the density is calculated so as to ensure energy conservation. The leakage mass flow rate is expressed by the formulation suggested by Denton [6] in the limit of incompressible leakage flow, where the leakage jet contraction effect is accounted for by means of a discharge coefficient. The direction of the leakage flow is assumed to be normal to the camber line of the tip section of the blade.

With this approach, the meridional flow distorsion effect associated with the tip leakage modelling is a result of the calculation and does not modify the prescribed S2 flow surface. It is then quite straightforward to identify the span fraction which is affected by the additional deviation due to the leakage flow. Once properly normalized, the deviation distribution can be adopted to represent the spanwise distribution of leakage losses. This is consistent with the assumption that such a loss contribution is concentrated where tip leakage effects are important. The corresponding entropy rise is obtained from correlations. In this work the one proposed by Yaras and Sjolander [21] has been used. A detailed description of the tip clearance model can be found in [13].

5. Radial Mixing model

Secondary and tip clearance flows are modelled in the throughflow method as additional 3D flow features whose effects are concentrated in selected regions of the meridional flowpath. This is not sufficient to ensure a realistic representation of the spanwise distributions of flow quantities. As discussed in several studies since three decades [1], the radial migration of the endwall flow plays a crucial role in determining the spanwise redistribution of flow distortions and losses in multistage turbomachinery.

A radial mixing model is therefore an important feature to be considered in a throughflow code. In the framework of the proposed methodology, the effect of mixing is introduced via diffusive terms in the momentum and energy equations. A Bousinnesq type assumption is adopted to express the stress tensor, where a mixing coefficient is used to calculate the eddy viscosity [7]. The thermal conductivity is then calculated using the Reynolds analogy. Only the stress components affecting the radial direction are retained in the formulation. Historically, two classes of models have been proposed for determining the mixing coefficient, ϵ: in the first case, it is supposed that a random, turbulent-type, diffusion process is the dominant mechanism (see Gallimore and Cumpsty [7]); in the second case, the spanwise redistribution process is supposed be completely deterministic and associated to secondary flows (see Adkins and Smith [1]). Finally, the work of Lewis [12], which is the one proposed in this paper, considers the spanwise transport due to secondary flows as superimposed to a background diffusion due to turbulence. The mixing coefficient is a function of the blade geometry, loss coefficient and secondary vorticity. It is defined as a field variable and, in multi-stage configurations, the contribution of each blade row is calculated separately and cumulated from the first to the last one. A Gaussian function is employed to define the inter blade distribution, so that the decay of the contribution of a given blade row is spread over 1.5 axial chords downstream.

Indeed, the mixing coefficient is related to the eddy viscosity by the Schmidt number, $Sc_t = \mu_t/(\rho\epsilon)$, and to the eddy thermal conductivity by the turbulent Prandtl number, $Pr_t = k_t/\left(\mu_t c_p\right)$. The experimental evidence suggests that Sc_t and Pr_t should be of the order of the unity [4]. Numerical experiments conducted over a range of multistage turbines have shown how a value of $Pr_t = 2.0$ gives radial distributions of total temperature that are in good agreement with 3D CFD results. The reliability of the proposed model has been confirmed in the present work as will be shown with aid of experimental data in the following section.

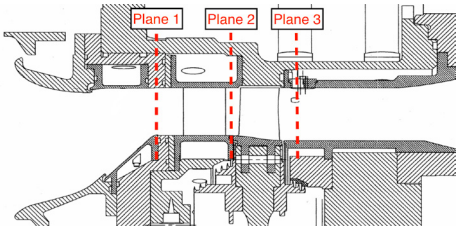

Fig. 1: Meridional view of the CT3 stage.

	$M_{2,is}$	$M_{3,is}$	p_{03}/p_{01}
Low	1.071	0.65	2.19
Nom	1.242	0.97	3.19
High	1.249	1.18	3.85

Table 1: Operating conditions for the CT3 stage.

6. Results

As a validation of the proposed methodology, the throughflow code was used to study the transonic CT3 turbine stage, which was experimentally tested at the *von Kármán Institute* in the framework of the TATEF2 European project. The turbine stage is composed by 43 cylindrical vanes and 64 unshrouded blades. A meridional view of the stage is reported in Figure 1. Three operating conditions (*Nominal*, *Low* and *High*) were investigated during the measurement campaign. Their isentropic Mach number at stator and rotor exit, and stage total pressure ratio are presented in Table 1. Experimental results are available for planes 1 and 3.

In the streamwise direction, the computational domain was discretized into 62 cells for each blade row, and about 46 cells for the inter-blade flow-paths. A number of 68 cells were used in the spanwise direction. The total grid size amounts to approximately 18,000 elements. A cell clustering was applied near leading edge and trailing edge in order to better represent the rapid variation of the blockage factor in those region.

The spanwise distributions of total temperature and total pressure at Plane 1 were used as inlet boundary conditions. The Kacker-Okapuu correlation was used to estimate profile deviations and losses.

In terms of radial distributions of flow quantities, throughflow results at the design condition are compared with experimental data and 3D, steady, viscous, CFD calculations obtained with the TRAF code [8], in Figures 2a, 2b, 2c, 2d. None of the simulations reproduces accurately the experimental spanwise distributions of all the flow quantities, but the level of agreement of the throughflow results with measured data is comparable with that of 3D CFD results, or even better for some quantities (i.e. absolute flow angle, total temperature). Indeed, the radial mixing model does a good job in improving the throughflow predictions near the endwalls but sensible discrepancies remain in the total pressure and absolute Mach number profiles: the strong distortions seen in experimental distributions and TRAF results in these regions are not captured. The same considerations can be repeated also for off-design conditions. The throughflow results for the *Low* and *High* conditions are compared to experiments and 3D CFD results in Figures 2e, 2f, 2g, 2h and 2i, 2j, 2k, 2l respectively. The overall good reproduction of the radial distributions of flow quantities observed for the nominal condition is conserved in the prediction of off-design operations of the turbine stage. Indeed, for the considered transonic, low aspect ratio configuration, the radial distributions of flow quantities undergo relevant changes when varying the stage expansion ratio. So, the scenario described by Figure 2 shows a remarkably accurate and reliable response of the proposed methodology to the changes in the tangentially averaged flow structure associated to different operating conditions for the stage.

The computed mass flow rate value is equal to $9.31 kg/s$ for all the three investigated operating conditions due to chocked flow in the vanes, and it is about 2% higher than the experimental value of $9.15 kg/s$. In terms of performance the comparison between computed and measured values is summarized in Figure 3. The calculated expansion ratio (Fig. 3a) and power (Fig. 3b) values are overestimated of about $2-3\%$ with respect to the experimental results and 3D CFD results. This is not surprising due the comparable overestimation in mass flow rate.

7. Conclusions

In this paper a novel, CFD-based throughflow method has been proposed. The computational method, which inherits its numerical scheme from a state-of-the-art Navier-Stokes solver, is complemented with a general framework for introducing the average effect of three-dimensional flow features in the context of the axisymmetric flow assumption. A radial mixing model, which account for background turbulent diffusion and deterministic spanwise transport due to

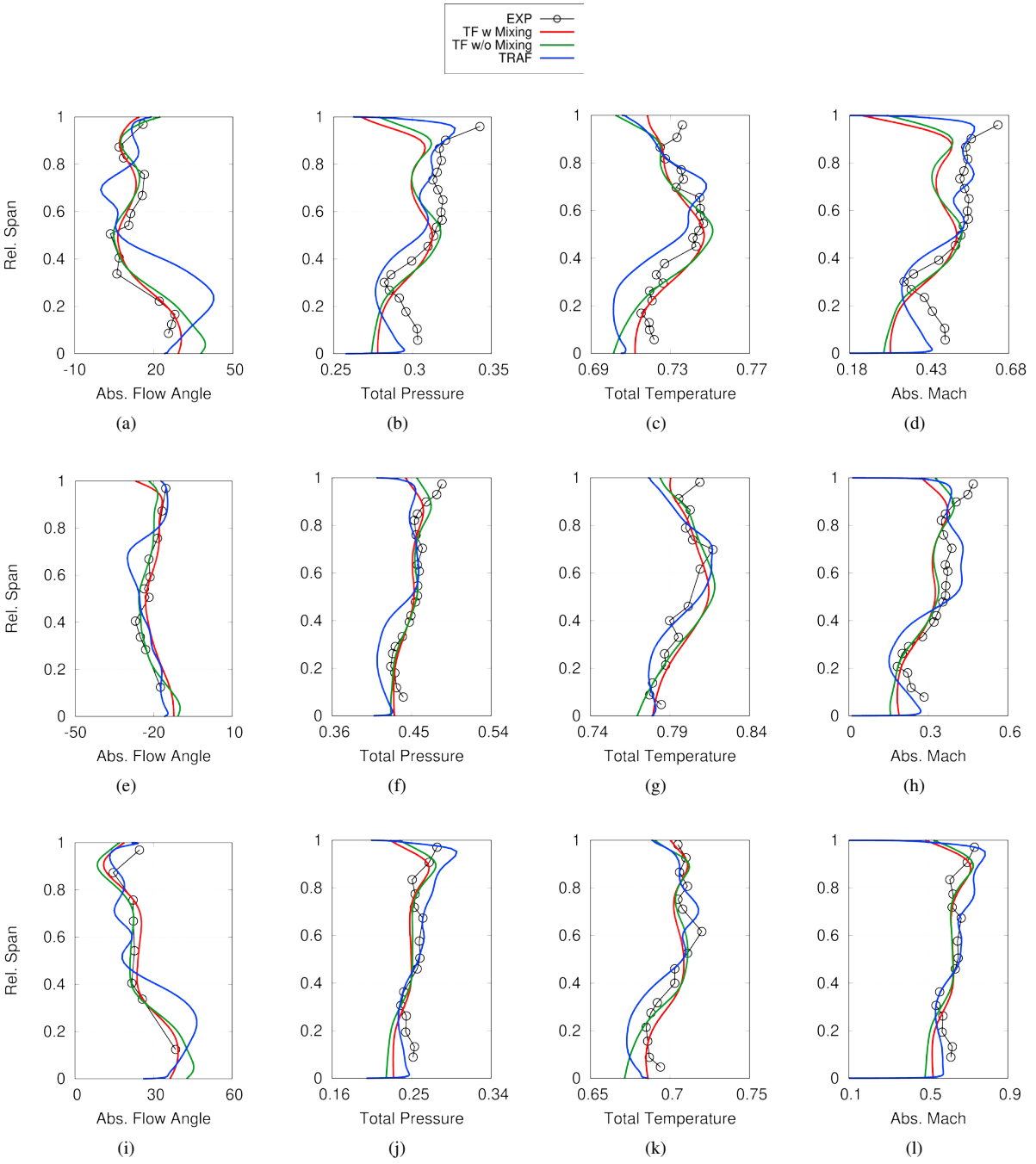

Fig. 2: Predicted and measured spanwise distributions of flow quantities in Plan 3 for the CT3 turbine stage at nominal (2a, 2b, 2c, 2d), low (2e, 2f, 2g, 2h) and high (2i, 2j, 2k, 2l) conditions with and without radial mixing effects.

secondary flows is also implemented. The accuracy and reliability of the method has been assessed by the application of the throughflow code to the analysis of the CT3 transonic turbine stage. The strong secondary flows occurring in this transonic, low aspect ratio turbine stage makes it a relevant test case to check for the capability of the code to reproduce the meridional flow structure in modern, highly loaded gas turbine stages. Calculated radial distributions of flow properties and stage performance were to found to be in good agreement with experiments not only at design

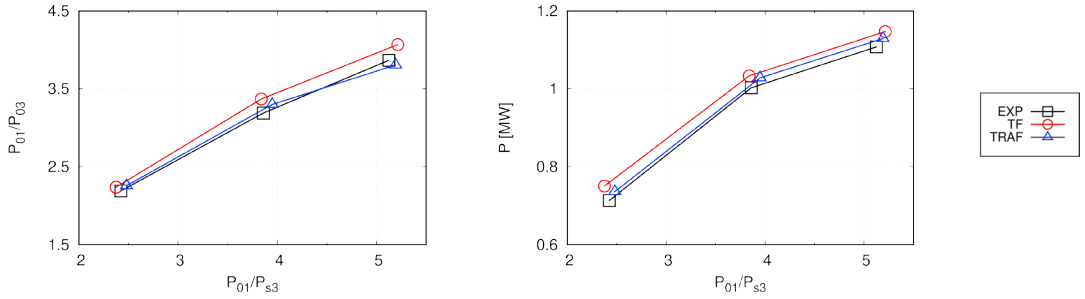

(a) (b)

Fig. 3: Measured and computed performance for the CT3 stage: (a) Total Pressure ratio; (b) Power.

conditions, but also when studying off design trends. It is believed that the performance of the proposed methodology is in line with the requirements of fast engineering predictions for the design of axial turbines.

Acknowledgements

The authors would like to thank all partners in European Union FP6 programme TATEF2 (Contract No. AST3-CT-2004-502924) for permitting the publication of their results in this paper.

References

[1] Adkins, G.G., Smith, L.H., 1982. Spanwise Mixing in Axial-Flow Turbomachines. J. of Engineering for Power 104, 97–110.
[2] Arnone, A., 1994. Viscous Analysis of Three-Dimensional Rotor Flow Using a Multigrid Method. J. Turbomach. 116, 435–445.
[3] Benner, M.W., Sjolander, S.A., Moustapha, S.H., 2006. An Empirical Prediction Method for Secondary Losses in Turbines - Part II: A New Secondary Loss Correlation. J. Turbomach. 128, 281–291.
[4] Bird, R.B., Stewart, W.E., Lightfoot, E.N., 1960. Transport Phenomena.
[5] Denton, J., 1978. Throughflow Calculations for Transonic Axial Flow Turbines. J. of Engineering for Power 100, 212–218.
[6] Denton, J., 1993. Loss Mechanisms in Turbomachines. J. Turbomach. 115, 621–656.
[7] Gallimore, S.J., Cumpsty, N.A., 1986. Spanwise Mixing in Multistage Axial Flow Compressors: Part I - Experimental Investigation. J. Turbomach. 108, 2–9.
[8] Giovannini, M., Marconcini, M., Arnone, A., Bertini, F., 2014. Evaluation of Unsteady Computational Fluid Dynamics Models Applied to the Analysis of a Transonic High-Pressure Turbine Stage. P. I. Mech. Eng. A-J. Pow. 228, 813–824.
[9] Hawthorne, W.R., Armstrong, W.D., 1955. Rotational Flow Through Cascades Part II. The Circulation About The Cascade. Q. Jl Mech. Appl. Math. 8, 280–292.
[10] Jameson, A., Schmidt, W., Turkel, E., et al., 1981. Numerical Solutions of the Euler Equations by Finite Volume Methods Using Runge-Kutta Time-Stepping Schemes. AIAA Paper 1259, 1981.
[11] Kacker, S.C., Okapuu, U., 1982. A Mean Line Prediction Method for Axial Flow Turbine Efficiency. J. of Engineering for Power 104, 111–119.
[12] Lewis, K.L., 1993. Spanwise Transport in Axial-Flow Turbines: Part 2 - Throughflow Calculations Including Spanwise Transport, in: ASME Turbo Expo, p. V03BT16A046.
[13] Pacciani, R., Marconcini, M., Arnone, A., 2017. A CFD-Based Throughflow Method with Three-Dimensional Flow Features Modelling. J. Turbomach., Propulsion and Power 2, 11.
[14] Pacciani, R., Rubechini, F., Marconcini, M., Arnone, A., et al., 2016. A CFD-Based Throughflow Method with An Adaptive Formulation For The S2 Streamsurface. P. I. Mech. Eng. A-J. Pow. 230, 16–28.
[15] Pasquale, D., Persico, G., Rebay, S., 2013. Optimization of Turbomachinery Flow Surfaces Applying a CFD-based Throughflow Method. J. Turbomach. 136, 031013.
[16] Rains, D.A., 1954. Tip Clearance Flows in Axial flow Compressors and Pumps. Ph.D. thesis. California Institute of Technology.
[17] Simon, J.F., Léonard, O., 2005. A Throughflow Analysis Tool based on the Navier–Stokes Equations, in: P. ETC6, pp. 7–11.
[18] Smith, L.H., 1966. The Radial-Equilibrium Equation of Turbomachinery. J. of Engineering for Power 88, 1–12.
[19] Sturrnayr, A., Hirsch, C., 1999. Shock Representation by Euler Throughflow Models and Comparison with Pitch-Averaged Navier-Stokes Solutions. Technical Report. ISABE 99–7281.
[20] Yao, Z., Hirsch, C.H., 1995. Throughflow Model Using 3D Euler or Navier-Stokes Solver. VDI Berichte 1185, 51–61.
[21] Yaras, I., Sjolander, S., 1992. Prediction of Tip-Leakage Losses in Axial Turbines. J. Turbomach. 114, 204–210.